JOURNAL OF THERMOPHYSICS AND HEAT TRANSFER
Vol. 11, No. 1, January–March 1997

Vibrationally Relaxing Flow of N_2 past an Infinite Cylinder

D. Giordano*
European Space Agency, Noordwijk 2200 AG, The Netherlands
V. Bellucci†
Center for Advanced Studies, Research and Development in Sardinia, Via Nazario Sauro 10, Cagliari, Italy
G. Colonna,‡ M. Capitelli,§ and I. Armenise‡
University of Bari, Bari 70126, Italy
and
C. Bruno¶
University of Rome I, Rome 00184, Italy

The results of a numerical study aimed to verify the accuracy of the thermodynamic models based on the Boltzmann distribution in the hypersonic regime and to detect discrepancies, if any, with the analysis based on the more rigorous method of vibrational kinetics are presented and discussed. The test case considered in the study is the steady, two-dimensional, chemically inert, inviscid flow of diatomic nitrogen past an infinite cylinder in a uniform stream at $M_\infty = 6.5$. The vibrational relaxation has been calculated from the standard vibrational energy rate equation, assuming a harmonic-oscillator behavior of N_2, and from a set of vibrational master equations that account for the first 10 vibrational energy levels of the N_2 molecule, assumed as an anharmonic oscillator. The flow patterns produced by the two calculation methods are thoroughly discussed and the critical influence of the vibrational relaxation time, associated with the harmonic-oscillator models, in determining agreement or disagreement with the results from the vibrational kinetics method is evidenced.

Nomenclature

A, B, C = constants in the relaxation time expression
c = speed of light, 2.998×10^8 m/s
e = total energy per unit mass
F, B = forward, backward rate coefficients
h = Planck constant, 6.626×10^{-34} J s
i, j = vibrational quantum numbers
l = number of vibrational levels
M = N_2 molecular mass, 0.0280134 kg/mole
M_∞ = asymptotic stream Mach number
N_A = Avogadro number, 0.602214×10^{24}
$\underline{\boldsymbol{n}}$ = cylinder normal unit vector
p = pressure
p_∞ = asymptotic stream pressure
R = N_2 gas constant, 296.797 J/kg K
R_G = universal gas constant, 8.3143 J/K
r = cylinder radius
$\underline{\boldsymbol{r}}$ = position vector
$\underline{\boldsymbol{r}}_{\text{cyl}}$ = position vector (cylinder)
T = translational temperature
T_{fl} = first-level temperature
T_v = vibrational temperature
T_∞ = asymptotic stream temperature
t = time
$\underline{\underline{U}}$ = isotropic tensor
u = thermodynamic energy per unit mass
u_{int} = internal thermodynamic energy per unit mass
u_r = rotational energy per unit mass
u_v = vibrational energy per unit mass
$\dot{u}_v$ = vibrational energy production
$\underline{\boldsymbol{v}}$ = velocity vector
$\underline{\Delta}$ = thermal disequilibrium parameter
ε_i = energy of the ith vibrational level
Θ_v = N_2 characteristic vibrational temperature, 3393 K
$\boldsymbol{\theta}$ = cylinder polar angle
$\dot{\Xi}_i^j, \dot{\Omega}_i^j$ = V–V exchange reaction velocities
$\dot{\boldsymbol{\xi}}_i, \dot{\omega}_i$ = V–T exchange reaction velocities
ρ = total mass density
ρ_i = partial density of the molecules on the ith vibrational level
$\dot{\rho}_i$ = mass production associated with the ith vibrational level
$(\dot{\rho}_i)^{\text{V–T}}$ = contribution of the V–T processes to $\dot{\rho}_i$
$(\dot{\rho}_i)^{\text{V–V}}$ = contribution of the V–V processes to $\dot{\rho}_i$
$\rho_{i,\infty}$ = asymptotic stream partial density of the molecules on the ith vibrational level
τ, τ_{vk} = relaxation time
ω_e = spectroscopic constant
$\omega_e x_e, \omega_e y_e$ = spectroscopic constants
$\underline{\nabla}$ = gradient operator

Introduction

THE thermodynamic models in use today in gasdynamics are constructed on the basic assumption that the population distributions (or probabilities) of the quantum states associated with each independent molecular degree of freedom follow a Boltzmann distribution. The major benefit derived from this hypothesis is that the thermodynamics of a gas mixture can be described by a set of algebraic functions, such as

Presented as Paper 95-2072 at the AIAA 30th Thermophysics Conference, San Diego, CA, June 19–22, 1995; received Dec. 15, 1995; revision received June 15, 1996; accepted for publication July 8, 1996.

*Research Engineer, Aerothermodynamics Section, P.O. Box 299. Member AIAA.
†Research Engineer, Group of Modeling of Combustion and Chemical Processes. Member AIAA.
‡Researcher, Centro di Studio per la Chimica dei Plasmi del CNR, Via Orabona 4, Dipartimento di Chimica.
§Professor of Chemistry, Centro di Studio per la Chimica dei Plasmi del CNR, Via Orabona 4, Dipartmento di Chimica.
¶Associate Professor, Mechanics and Aeronautics Department, Via Eudossiana 18. Member AIAA.

fundamental relations and/or state equations. The thermodynamic models built on the Boltzmann distribution have never been questioned in the engineering applications of the subsonic and supersonic regimes because their accuracy has always been experimentally verified; it is, therefore, understandable how the same assumption has been favorably used also to construct thermodynamic models and to produce tables of thermodynamic properties needed in applications of pertinence to the hypersonic regime. However, the energy densities of the flowfield become considerably large for sufficiently high Mach numbers and lead to more marked nonequilibrium effects; therefore, one should expect the Boltzmann distribution assumption to become less tenable under those circumstances. Nonetheless, the applicability in the hypersonic regime of the thermodynamic models based on the Boltzmann distribution has always been tacitly admitted in the vast majority of the fluid dynamics community for obvious reasons of convenience when practical calculations of realistic flowfields are called for. On the other hand, some researchers have expressed the opinion that the confidence about the accuracy of the results may sometimes be not as secure as in the case of the subsonic and supersonic regimes.

A more fundamental and rigorous approach to the problem is to calculate the population distributions from the master equations[1–4] governing the kinetics of the particle exchanges among the quantum states. In principle, this idea applies indistinctly to any molecular degree of freedom. However, attention in the literature has been prevalently focused on the vibrational degree of freedom, with particular concern to the diatomic molecules; thus, the term vibrational kinetics has come into use to refer to the subject. In this approach, thermodynamics and gasdynamics are inseparably coupled, because, in a gasdynamical context, the master equations assume the form of balance equations just like those of mass, momentum, and energy. Unfortunately, such a rigorous approach is affected by a major impediment of computational nature: the integration of the huge number of differential equations required for the analysis of a realistic case, for example, the hypersonic airflow past a re-entry vehicle configuration, within the computation times imposed by a typical design process is far beyond the reach of the computer power available today.

One is, thus, confronted with a conflicting situation: on one hand there is the necessity to produce accurate calculations of realistic hypersonic flowfields in reasonably affordable computation times, whereas on the other hand, there is the constraint that, for the time being, the computational time requirements may be met by only relying on the thermodynamic models based on the Boltzmann distribution, a working assumption whose validity may sometimes appear questionable. Such a situation clearly points out the need to investigate and understand if and to what extent these thermodynamic models are applicable in the hypersonic regime. In the authors' opinion, a reasonable manner to achieve such an understanding is to define relatively simple but meaningful test cases, for which the computational load imposed by the master equations can still be within the reach of modern computers, and to study them by using both the traditional thermodynamic models and the rigorous approach based on the master equations. Hopefully, the comparison of the results produced by the two methods for a series of test cases covering the critical aspects of the problem should yield valuable information, particularly when backed by experimental data, which would constitute the useful background necessary when more realistic applications of the engineering practice are dealt with.

Researchers have been aware of the necessity to pursue such an investigation since the sixties, but efforts[5–12] in that direction are still under way today. The work described in this article is meant to contribute to those efforts, and it consists of a thorough discussion of the flow patterns past an infinite cylinder in a hypersonic stream of N_2 produced by the two calculation methods. In particular, the critical influence of the vibrational relaxation time, relative to the harmonic-oscillator models, in determining accordance with the results from the vibrational kinetics method is evidenced in the relevant diagrams.

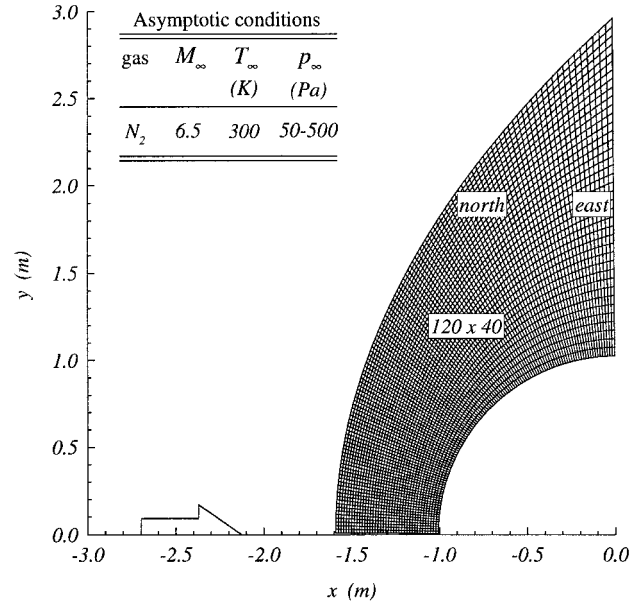

Fig. 1 Flow configuration and computational mesh.

Description of the Test Case

The test case we have studied numerically is the steady, two-dimensional, chemically inert, inviscid flow at $M_\infty = 6.5$ of N_2 past an infinite cylinder of radius $r = 1$ m in a hypersonic uniform stream. The stream is considered in thermal equilibrium. A sketch of the flow configuration, together with the computational mesh and the stream conditions, is given in Fig. 1.

The main reasons behind our choice are the following:

1) The flow pattern in the stagnation region behind the bow shock is representative of blunt body flows and, therefore, it is of specific relevance to re-entry aerothermodynamics.

2) The possibility to analyze in a single test case both compression and expansion regions.

Our main objective was to verify the accuracy of the thermodynamic models constructed on the Boltzmann distribution and to detect discrepancies, if any, with the results from the more rigorous method of vibrational kinetics. As a first step in the analysis of the problem, viscosity and thermal conduction effects have been disregarded; moreover, the T_∞ was set to 300 K to keep, for the assumed $M_\infty = 6.5$, the translational temperature peak below 3000 K in the flow region behind the shock wave: this bound guarantees a complete chemically inert behavior of N_2. Calculations have been performed for a p_∞ of 50 and 500 Pa with the intent to favor thermal disequilibrium in the former case and thermal equilibrium in the latter one.

In line with our main objective, the vibrational relaxation has been calculated from the standard vibrational energy rate equation, assuming a harmonic-oscillator behavior of N_2, and from a set of vibrational master equations that account for the first 10 vibrational energy levels of the N_2 molecule, assumed as an anharmonic oscillator. The expressions of the relaxation time proposed by Millikan and White[13] and Blackman[14] have been used when the traditional harmonic-oscillator model was assumed for N_2.

Governing Equations

Basic Equations

Consistent with the assumption of negligible viscosity and thermal conduction effects, and in the absence of body forces,

the balance equations of mass, momentum, and total energy in conservation form read

$$\frac{\partial \boldsymbol{\rho}}{\partial t} + \underline{\nabla}\cdot(\boldsymbol{\rho}\underline{\boldsymbol{v}}) = 0 \tag{1}$$

$$\frac{\partial \rho \underline{\boldsymbol{v}}}{\partial t} + \underline{\nabla}\cdot(\rho \underline{\boldsymbol{v}}\underline{\boldsymbol{v}} + p\underline{\underline{U}}) = 0 \tag{2}$$

$$\frac{\partial \rho e}{\partial t} + \underline{\nabla}\cdot\left[\rho\left(e + \frac{p}{\rho}\right)\underline{\boldsymbol{v}}\right] = 0 \tag{3}$$

The total energy comprises u and the kinetic energy $v^2/2$

$$e = u + (v^2/2) \tag{4}$$

In turn, the thermodynamic energy is made up by the translational and the internal parts

$$u = \tfrac{3}{2}RT + u_{\text{int}} \tag{5}$$

For a diatomic molecule far from dissociation, the internal part u_{int} can be satisfactorily separated in a rotational and a vibrational contribution

$$u_{\text{int}} = u_r + u_v \tag{6}$$

This situation is expected to exist throughout the whole flowfield as a consequence of the purposely chosen conditions of the asymptotic stream.

The N_2 molecule is assumed to behave as a rigid rotator and the population distribution over its rotational quantum states is assumed to follow a Boltzmann distribution. Moreover, the corresponding rotational temperature is taken equal to the translational one; in other words, mutual thermal equilibrium is assumed to exist between the translational and the rotational degrees of freedom. Consistently, the rotational contribution to the thermodynamic energy is

$$u_r = RT \tag{7}$$

and Eq. (4) can be expanded to read

$$e = \tfrac{5}{2}RT + u_v + (v^2/2) \tag{8}$$

Equation (8) is used to determine the translational temperature.

The thermodynamic pressure is not affected by the internal degrees of freedom and is given in terms of the translational temperature according to the standard expression

$$p = \rho RT \tag{9}$$

The set of Eqs. (1–3), (8), and (9) is shared by both calculation methods. The basic feature that distinguishes the methods consists of the approach used to determine the vibrational energy.

Harmonic–Oscillator Model

When the N_2 molecule is assumed to behave as a harmonic oscillator, the population distribution over its vibrational quantum states follows a Boltzmann distribution characterized by a vibrational temperature, which, in general, differs from the translational one when thermal disequilibrium prevails. Accordingly, the vibrational contribution to the thermodynamic energy is

$$u_v = \frac{R\Theta_v}{\exp(\Theta_v/T_v) - 1} \tag{10}$$

Equation (10) is used to calculate the vibrational temperature.

Table 1 Relaxation time constants

Source	A, atm s	B, $K^{1/3}$	C
Ref. 14	7.12×10^{-9}	124.07	0
Ref. 13	1	221.35	−24.84

Consistent with the assumption of negligible thermal conduction effects, the balance equation of the vibrational energy reads

$$\frac{\partial \rho u_v}{\partial t} + \underline{\nabla}\cdot(\rho u_v \underline{\boldsymbol{v}}) = \rho \dot{u}_v \tag{11}$$

In accordance with the harmonic–oscillator vibrational relaxation theory,[15,16] the production term on the right-hand side (RHS) of Eq. (11) reads

$$\dot{u}_v = \frac{u_v^* - u_v}{\tau} \tag{12}$$

On the RHS of Eq. (12), u_v^* is the vibrational energy attained in case of thermal equilibrium at the local translational temperature; by definition, this energy is obtained from Eq. (10), simply by replacing T_v with T:

$$u_v^* = \frac{R\Theta_v}{\exp(\Theta_v/T) - 1} \tag{13}$$

The relaxation time τ is determined from the expression[15,16]

$$\tau = (A/p)\exp[(B/T^{1/3}) + C] \tag{14}$$

which is an approximate form of the one derived in the Landau and Teller's theory. The constants A or C and B are found, in practice, by fitting Eq. (14) to experimental data. The sets of constants (see Table 1) proposed by Millikan and White[13] and Blackman[14] have been used in this study. A substantial discrepancy[17] exists between these sources. In particular, the relaxation time corresponding to Millikan and White's[13] constants is systematically greater than the one determined by Blackman's[14] constants, at any given pressure; therefore, the vibrational relaxation driven by Millikan and White's[13] relaxation time should be expected appreciably slower than the one driven by the relaxation time proposed by Blackman.[14]

Vibrational Kinetics Model

In this model, the populations of the vibrational quantum states are unknowns of the problem and have to be determined via the master equations governing the kinetics of the particle exchanges among those states. In a fluid dynamics context, the master equations assume the role of balance equations for the masses distributed over the vibrational quantum levels; they read

$$\frac{\partial \rho_i}{\partial t} + \underline{\nabla}\cdot(\rho_i \underline{\boldsymbol{v}}) = \dot{\rho}_i \qquad i = 1, \ldots, l \tag{15}$$

The diffusion term has been neglected on the RHS of Eq. (15) for consistency with the absence of viscosity and thermal conduction terms in Eqs. (2) and (3). The summation of the partial densities yields the total mass density

$$\sum_{i=1}^{l} \rho_i = \rho \tag{16}$$

and the summation of the production terms vanishes identically

$$\sum_{i=1}^{l} \dot{\rho}_i = 0 \tag{17}$$

Table 2 Spectroscopic constants, m^{-1}

ω_e	$\omega_e x_e$	$\omega_e y_e$
235,857	1432.4	−0.226

for congruence with the total mass conservation. Accordingly, the summation over the subscript i of Eq. (15) returns the mass balance equation [Eq. (1)]. Therefore, one can either use the l equations [Eq. (15)], relinquish Eq. (1), and calculate the total mass density from Eq. (16); or use $l - 1$ equations [Eq. (15)], retain Eq. (1), and calculate the missing partial density from Eq. (16). We have adopted the former scheme.

The vibrational energy is calculated as

$$u_v = \frac{N_A}{M} \sum_{i=1}^{l} \frac{\rho_i}{\rho} \varepsilon_i \tag{18}$$

The ratio ρ_i/ρ on the RHS of Eq. (18) represents the population of the ith vibrational level. The quantum level energies ε_i are determined from the third-order approximating formula[18]:

$$\varepsilon_i/hc = \omega_e(i - \tfrac{1}{2}) - \omega_e x_e(i - \tfrac{1}{2})^2 + \omega_e y_e(i - \tfrac{1}{2})^3 \qquad i = 1, 2, \ldots \tag{19}$$

The spectroscopic constants appearing in Eq. (19) are given by Huber and Herzberg[19] and are listed in Table 2. Equation (19) reflects an anharmonic–oscillator behavior of the N_2 molecule; in fact, the vibrational quantum is not constant and decreases with increasing quantum number. The spectrum generated from Eq. (19) is truncated when the value of the energy becomes greater than the N_2 dissociation energy (9.62 eV = 1.541×10^{-18} J); this occurs[11,12] when $i = 45$, but the computational load becomes very heavy if all of those levels are taken into account. However, for the particular flow conditions assumed in this study, i.e., the absence of dissipative effects and of chemical activity of N_2, preliminary calculations have shown that there are no substantial differences in the results if a reduced number of levels is considered; according to preliminary results, the choice $l = 10$ appears a reasonable compromise between the accuracy deriving from considering the whole vibrational spectrum, i.e., $l = 45$, and the necessity to deal with affordable computational loads.

The production terms $\dot{\rho}_i$ are associated with the kinetic mechanisms according to which the particle exchanges among the quantum states take place. There are two kinds of processes relevant to the case considered in this study: V–T processes, in which a molecule loses or gains a vibrational quantum as a result of a collision with another molecule, and V–V processes, in which a vibrational quantum is exchanged between the colliding molecules. The production term $\dot{\rho}_i$ is given by the sum of the contributions corresponding to these two processes:

$$\dot{\rho}_i = (\dot{\rho}_i)^{V-T} + (\dot{\rho}_i)^{V-V} \tag{20}$$

Processes V–T

The V–T exchange reactions responsible for the variation of the particles distributed on the ith vibrational level are

$$N_2(i + 1) + N_2 \rightleftharpoons N_2(i) + N_2 \qquad i = 1, \ldots, l - 1 \tag{21}$$

$$N_2(i) + N_2 \rightleftharpoons N_2(i - 1) + N_2 \qquad i = 2, \ldots, l \tag{22}$$

The contribution $(\dot{\rho}_i)^{V-T}$ is proportional to the difference of the reaction velocities $\dot{\xi}_i$ and $\dot{\omega}_i$, corresponding to, respectively, the replenishing and depleting processes [Eqs. (21) and (22)]; it reads

$$(\dot{\rho}_i)^{V-T} = M(\dot{\xi}_i - \dot{\omega}_i) \qquad i = 2, \ldots, l - 1 \tag{23}$$

Table 3 Relaxation time constants from the vibrational kinetics method

A, atm s	B, $K^{1/3}$	C
1	179.43	−22.78

The replenishing reaction [Eq. (21)] is the only one applicable to the ground state

$$(\dot{\rho}_1)^{V-T} = M\dot{\xi}_1 \tag{24}$$

whereas the depleting reaction [Eq. (22)] is the only one applicable to the last quantum level

$$(\dot{\rho}_l)^{V-T} = -M\dot{\omega}_l \tag{25}$$

The reaction velocities are given in terms of the partial densities according to the standard rate expressions

$$\dot{\xi}_i = F_{i+1,i} \frac{\rho_{i+1}}{M} \frac{\rho}{M} - B_{i,i+1} \frac{\rho_i}{M} \frac{\rho}{M} \qquad i = 1, \ldots, l - 1 \tag{26}$$

$$\dot{\omega}_i = F_{i,i-1} \frac{\rho_i}{M} \frac{\rho}{M} - B_{i-1,i} \frac{\rho_{i-1}}{M} \frac{\rho}{M} \qquad i = 2, \ldots, l \tag{27}$$

The B coefficients on the RHS of Eqs. (26) and (27) are calculated from the F coefficients according to the formula

$$B_{i-1,i} = F_{i,i-1} \exp\left(-\frac{\varepsilon_i - \varepsilon_{i-1}}{kT}\right) \qquad i = 2, \ldots, l \tag{28}$$

which derives from equilibrium considerations applied to the V–T exchange reactions [Eqs. (21) and (22)]. The forward rate coefficients, in turn, are calculated according to the expressions proposed by Capitelli et al.[20] and by Billing and Fisher[21]; they read

$$F_{i,i-1} = (i - 1)f(T)\exp[(i - 2)\delta(T)] \qquad i = 2, \ldots, l \tag{29}$$

where

$$f(T) = 10^{-6} N_A \exp[-3.24093 - (140.69597/T^{0.2})] \tag{30}$$

$$\delta(T) = 0.26679 - 6.99237 \times 10^{-5} T + 4.70073 \times 10^{-9} T^2 \tag{31}$$

The translational temperature on the RHS of Eqs. (30) and (31) must be in degrees Kelvin; in this way the forward rate coefficients returned from Eq. (29) have the units m^3/mole s.

The vibrational kinetics method does not require the introduction of a relaxation time. However, for reasons of comparison with Eq. (14), in use with the harmonic–oscillator models, a characteristic relaxation time τ_{vk} can be defined in terms of the coefficient $F_{2,1}$ as

$$\tau_{vk} = \frac{1}{p} \frac{R_G T}{F_{2,1}[1 - \exp[-(\Theta_v/T)]]} \tag{32}$$

The coefficient $F_{2,1}$ is more commonly denoted with the symbol $K_{1,0}$. The associated vibrational relaxation parameter $p\tau_{vk}$ is found in remarkable agreement[17] above 1500 K, with the parameter $p\tau$ from Eq. (14) corresponding to Blackman's[14] constants. The values obtained from Eq. (32) have been fitted to Eq. (14); the relative constants are listed in Table 3.

Processes V–V

In the case of the V–V processes, the reactions responsible

for the variation of the particles distributed on the ith vibrational level are

$$\begin{gathered} N_2(i+1) + N_2(j-1) \rightleftharpoons N_2(i) + N_2(j) \\ [(\forall i{:}\ j = 2, \ldots, l) \quad i = 1, \ldots, l-1] \end{gathered} \tag{33}$$

$$\begin{gathered} N_2(i) + N_2(j-1) \rightleftharpoons N_2(i-1) + N_2(j) \\ [(\forall i{:}\ j = 2, \ldots, l) \quad i = 2, \ldots, l] \end{gathered} \tag{34}$$

The contribution $(\dot{\boldsymbol{\rho}}_i)^{\mathrm{V-V}}$ is proportional to the sum, on j, of the differences of $\dot{\Xi}_i^j$, $\dot{\Omega}_i^j$ associated with, respectively, the replenishing and depleting processes [Eqs. (33) and (34)]; it reads

$$(\dot{\boldsymbol{\rho}}_i)^{\mathrm{V-V}} = M \sum_{j=2}^{l} (\dot{\Xi}_i^j - \dot{\Omega}_i^j) \qquad i = 2, \ldots, l-1 \tag{35}$$

Again, the replenishing reactions [Eq. (33)] are the only ones applicable to the ground state

$$(\dot{\rho}_1)^{\mathrm{V-V}} = M \sum_{j=2}^{l} \dot{\Xi}_1^j \tag{36}$$

and the depleting reactions [Eq. (34)] are the only ones applicable to the last quantum level

$$(\dot{\rho}_l)^{\mathrm{V-V}} = -M \sum_{j=2}^{l} \dot{\Omega}_l^j \tag{37}$$

The rate expressions of $\dot{\Xi}_i^j$, $\dot{\Omega}_i^j$ in terms of the partial densities read

$$\begin{gathered} \dot{\Xi}_i^j = F_{i+1,i}^{j-1,j} \frac{\rho_{i+1}}{M} \frac{\rho_{j-1}}{M} - B_{i,i+1}^{j,j-1} \frac{\rho_i}{M} \frac{\rho_j}{M} \\ [(\forall i{:}\ j = 2, \ldots, l) \quad i = 1, \ldots, l-1] \end{gathered} \tag{38}$$

$$\begin{gathered} \dot{\Omega}_i^j = F_{i,i-1}^{j-1,j} \frac{\rho_i}{M} \frac{\rho_{j-1}}{M} - B_{i-1,i}^{j,j-1} \frac{\rho_{i-1}}{M} \frac{\rho_j}{M} \\ [(\forall i{:}\ j = 2, \ldots, l) \quad i = 2, \ldots, l] \end{gathered} \tag{39}$$

Equilibrium considerations applied to the V–V exchange reactions [Eqs. (33) and (34)] lead to the formula

$$\begin{gathered} B_{i-1,i}^{j,j-1} = F_{i,i-1}^{j-1,j} \exp\left(-\frac{\varepsilon_i - \varepsilon_{i-1} + \varepsilon_{j-1} - \varepsilon_j}{kT}\right) \\ [(\forall i{:}\ j = 2, \ldots, l) \quad i = 2, \ldots, l] \end{gathered} \tag{40}$$

which gives the backward rate coefficients in terms of the forward rate coefficients; these, in turn, are calculated according to the formula given by Doroshenko et al.[22]

$$\begin{aligned} F_{i,i-1}^{j-1,j} &= 2.5 \times 10^{-20} N_A (i-1)(j-1) \\ &\times (T/300)^{3/2} \exp[-(6.8/\sqrt{T})|i-j|][1.5 - 0.5 \\ &\times \exp[-(6.8/\sqrt{T})|i-j|]] \\ &[(\forall i{:}\ j = 2, \ldots, l) \quad i = 2, \ldots, l] \end{aligned} \tag{41}$$

which is symmetric with respect to i, j. The forward rate coefficients returned from Eq. (41) have units m^3/mole s, if the translational temperature is in degrees Kelvin.

Initial and Boundary Conditions

The initial conditions ($t = 0$) assumed for the calculation of the flowfield correspond to those of the asymptotic stream

$$\begin{gathered} \underline{\boldsymbol{v}}(\underline{\boldsymbol{r}}, 0) = \underline{\boldsymbol{v}}_\infty \\ p(\underline{\boldsymbol{r}}, 0) = p_\infty \\ T(\underline{\boldsymbol{r}}, 0) = T_\infty \end{gathered}$$

In the case of the vibrational kinetics, the partial densities are initialized to the values corresponding to a Boltzmann distribution, at the temperature T_∞, on the first l levels of the spectrum produced by Eq. (19); thus

$$\rho_i(\underline{\boldsymbol{r}}, 0) = \rho_{i,\infty} \qquad i = 1, \ldots, l \tag{42}$$

with

$$\frac{\rho_{i,\infty}}{\rho_\infty} = \exp\left(\frac{\varepsilon_i}{kT_\infty}\right) \Big/ \sum_{j=1}^{l} \exp\left(\frac{\varepsilon_j}{kT_\infty}\right) \qquad i = 1, \ldots, l \tag{43}$$

The denominator on the RHS of Eq. (43) represents the associated partition function. The asymptotic density ρ_∞ is found from asymptotic pressure and temperature via the state equation [Eq. (9)].

The boundary conditions at infinity coincide with the initial conditions

$$\begin{gathered} \underline{\boldsymbol{v}}(\infty, t) = \underline{\boldsymbol{v}}_\infty \\ p(\infty, t) = p_\infty \\ T(\infty, t) = T_\infty \\ \rho_i(\infty, t) = \rho_{i,\infty} \qquad i = 1, \ldots, l \end{gathered} \tag{44}$$

The boundary conditions [Eq. (44)] are, in practice, imposed on the north boundary of the grid (see Fig. 1). Furthermore, the x axis is a line of symmetry and, consistent with the assumption of absent viscosity, the cylinder contour is a streamline:

$$\underline{\boldsymbol{n}} \cdot \underline{\boldsymbol{v}}(\underline{\boldsymbol{r}}_{\mathrm{cyl}}, t) = 0 \tag{45}$$

Finally, the variables $\underline{\boldsymbol{v}}$, p, T, and ρ_i ($i = 1, \ldots, l$) on the east boundary of the grid are obtained from a first-order extrapolation.

Numerical Scheme

The system of governing Eqs. (1–3) and (11), or (2), (3), and (15), can be synthetically written

$$\frac{\partial \mathbf{W}}{\partial t} + \nabla \cdot \mathbf{f} = \mathbf{H} \tag{46}$$

The numerical discretization is obtained by a cell-centered, finite volume method, and the system [Eq. (46)] is integrated over an elemental volume of the computational domain by a central difference scheme. The adaptive dissipation model[23] is included; this model uses a blend of second and fourth differences: the former prevent oscillations near the location of shock waves, the latter are important for stability and convergence to steady state.

The scheme is second-order accurate in space on Cartesian grids. The time integration is performed by a five-stage Runge–Kutta scheme.

Discussion of the Results

Stagnation Line

The stagnation line is a zone of strong compression.[17] The pressure raises across the shock wave to about 50 times the asymptotic pressure, and the ratio p/p_∞ increases further downstream up to the value 55 at the stagnation point. The different models predict approximately the same pressure profile, although the harmonic–oscillator model with Millikan and White's[13] relaxation time produces a slightly larger standoff distance.[17]

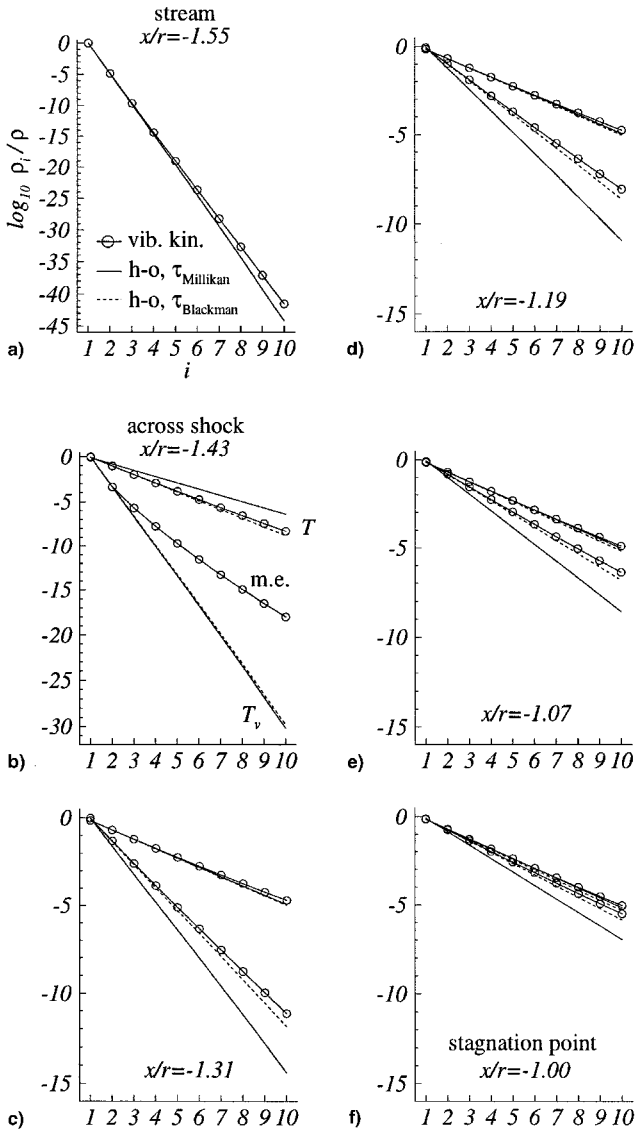

Fig. 2 Population distributions over the vibrational levels at stations along the stagnation line. p_∞ = 50 Pa.

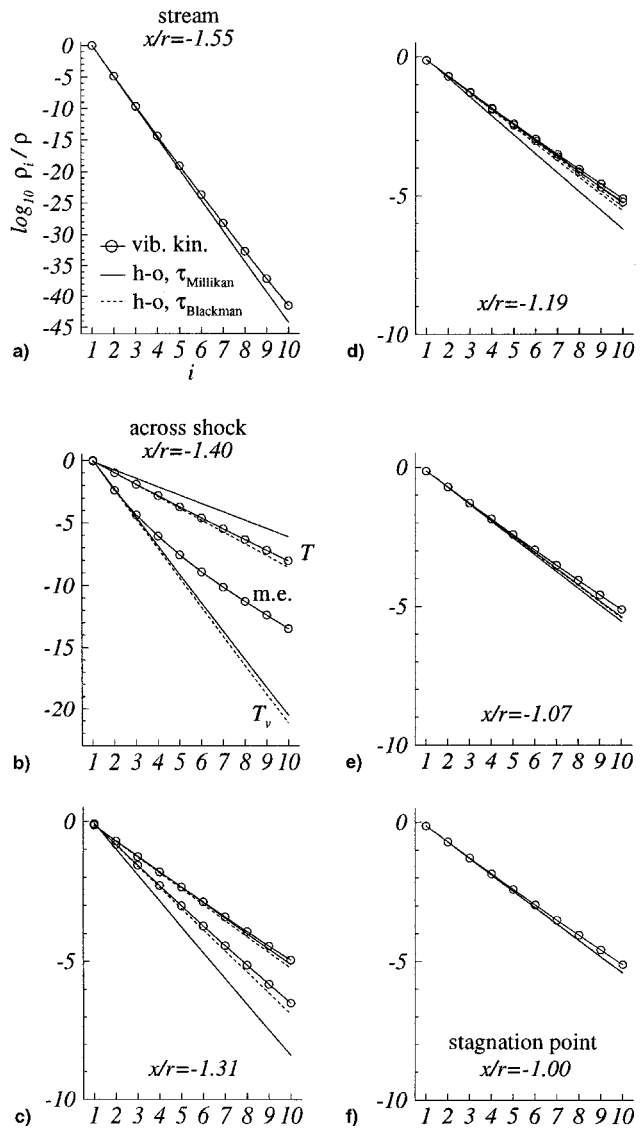

Fig. 3 Population distributions over the vibrational levels at stations along the stagnation line. p_∞ = 500 Pa.

The population distributions over the vibrational energy levels at various stations along the stagnation line are shown in Figs. 2 and 3; these figures illustrate the vibrational relaxation of the generic fluid particle during its travel to the stagnation point. The plain solid and dashed lines refer to the harmonic–oscillator model with, respectively, Millikan and White's[13] and Blackman's[14] relaxation time; their lack of curvature is a typical characteristic derived from the harmonicity of the oscillator model. The solid lines with circles are relative to the vibrational kinetics model. The lower three lines (refer to Figs. 2b and 3b for a clearer view) describe the vibrational relaxation. The lower plain solid and dashed lines (marked with T_v in Figs. 2b and 3b) are determined by the vibrational temperatures associated with the two harmonic–oscillator models at that particular station, and are found from

$$\frac{\rho_i}{\rho} = \frac{\exp[-(i-1)(\Theta_v/T_v)]}{[1-\exp[-(\Theta_v/T_v)]]^{-1}} \qquad i = 1, 2, \ldots \qquad (47)$$

The denominator on the RHS of Eq. (47) is the harmonic–oscillator partition function.[15] The lower solid circled line (marked m.e. in Figs. 2b and 3b) is the population distribution produced by the master equations [Eq. (15)]. The upper three lines (marked with T in Figs. 2b and 3b) are the distributions based on the translational temperatures associated with each model at that particular station. In the case of the harmonic–oscillator models, they are found from Eq. (47) by simply replacing T_v with the corresponding T; in the case of the vibrational kinetics, the distribution is found from

$$\frac{\rho_i}{\rho} = \exp\left(\frac{\varepsilon_i}{kT}\right) \Big/ \sum_{j=1}^{10} \exp\left(\frac{\varepsilon_j}{kT}\right) \qquad i = 1, \ldots, 10 \qquad (48)$$

which is a Boltzmann distribution on the first 10 levels of the spectrum produced by Eq. (19). The distance between lines of the same style or, better, the difference in their slopes, is indicative of how the corresponding model predicts the thermal disequilibrium.

Figures 2a and 3a reflect the situation in the asymptotic stream, where thermal equilibrium prevails, i.e., $T = T_v = T_\infty$. Thus, lower and upper families of lines coincide; moreover, the plain solid and dashed lines are obviously superposed. The slight curvature shown by the solid circled line is caused by the anharmonicity of the energy levels derived from Eq. (19); the curvature disappears if the populations are plotted vs the energy of the levels rather than the vibrational quantum number.

Figures 2b and 3b illustrate the situation across the shock wave. In the context of the harmonic–oscillator models, the

translational and vibrational temperatures differ, as shown by the different slopes of the corresponding plain solid and dashed lines; in the context of the vibrational kinetics model, the population distribution produced by the master equations (line marked m.e.) differs from the Boltzmann distribution at the corresponding translational temperature (upper solid circled line) and becomes non-Boltzmann from the third vibrational level when p_∞ = 50 Pa, and from the fourth vibrational level when p_∞ = 500 Pa.

Figures 2c–2f and 3c–3f show the relaxation toward thermal equilibrium: the lower three lines tend to superpose to the upper three lines. However, in the low asymptotic pressure case, the standoff distance is not sufficient to allow the achievement of thermal equilibrium at the stagnation point; on the contrary, the thermal equilibrium is fully achieved somewhere upstream of the stagnation point in the high asymptotic pressure case. Furthermore, in both cases the population distributions predicted by the master equations coincide satisfactorily with a Boltzmann distribution downstream of the shock wave, at least for the 10 levels accounted for in this study, and they are found to be in substantial agreement with the Boltzmann distributions derived from the harmonic–oscillator model with Blackman's[14] relaxation time. The harmonic–oscillator model with Millikan and White's[13] relaxation time, instead, overestimates systematically the thermal disequilibrium with respect to the other models.

The conclusions drawn from the diagrams of Figs. 2 and 3 are confirmed by those (of more fluid dynamics nature) of Figs. 4 and 5, which show the profiles along the stagnation line of the nondimensional translational, vibrational, and first-level temperatures. The vibrational kinetics model does not require the introduction of a vibrational temperature. However, a first-level temperature can be introduced for the convenience of comparing results in terms of temperatures. The first-level temperature is defined as the temperature corresponding to the Boltzmann distribution, which can be accommodated on the population ρ_1/ρ of the first vibrational level. In the present study, therefore, it was calculated by solving the equation

$$\frac{\rho_1}{\rho} = \exp\left(\frac{\varepsilon_1}{kT_{f1}}\right) \Big/ \sum_{j=1}^{10} \exp\left(\frac{\varepsilon_j}{kT_{f1}}\right)$$

with respect to T_{f1}.

Cylinder Wall

The cylinder wall is a zone of strong expansion,[17] where the nondimensional pressure drops from 55 at the stagnation point to 5 at the cylinder top.

The population distributions over the vibrational energy levels at the stagnation point and cylinder top are shown in Figs. 6 and 7; in these figures, the line style convention adopted for Figs. 2 and 3 applies again. Figures 6a and 7a are a copy of Figs. 2f and 3f; they have been replotted in a different scale for convenience of comparison. Figures 6b and 7b show the situation at the cylinder top: the expansion along the cylinder wall brings the vibrational relaxation lines to overshoot the lines based on the translational temperatures. Here again, the population distributions produced by the master equations coincide satisfactorily with a Boltzmann distribution.

The diagrams of Figs. 8 and 9 yield a clear understanding of the vibrational relaxation along the cylinder wall. In the low asymptotic pressure case (see Fig. 8), no spatial region of thermal equilibrium exists; the vibrational and first-level temperatures overshoot the corresponding translational temperatures in a single point, i.e., the point of thermal equilibrium, which is predicted at an angular position $\theta \cong 45$ deg by the vibrational kinetics model and the harmonic–oscillator model with Blackman's[14] relaxation time, and at an angular position $\theta \cong 74$ deg by the harmonic–oscillator model with Millikan and White's[13] relaxation time. Once again, this latter model overestimates the thermal disequilibrium with respect to the former

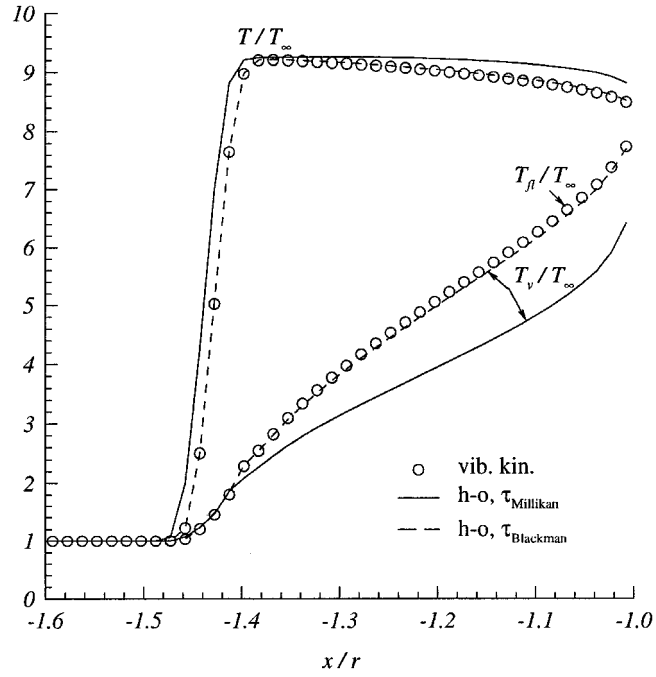

Fig. 4 Nondimensional translational, vibrational, and first-level temperature profiles along the stagnation line. p_∞ = 50 Pa.

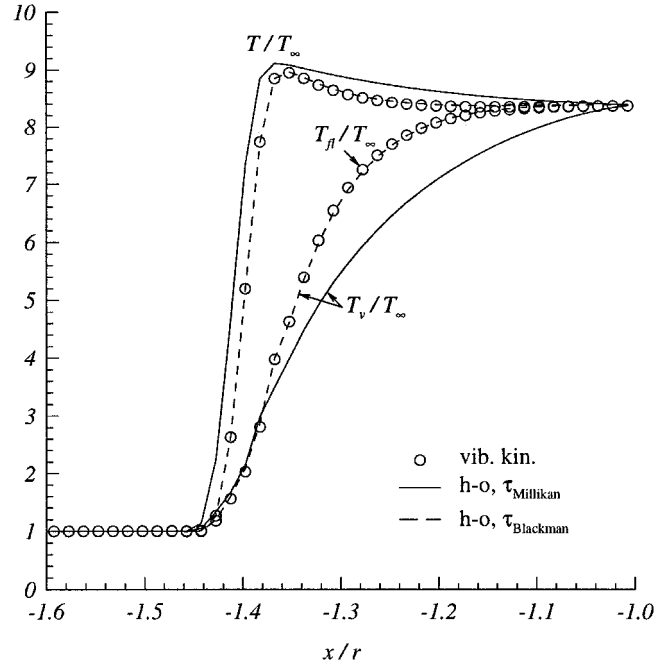

Fig. 5 Nondimensional translational, vibrational, and first-level temperature profiles along the stagnation line. p_∞ = 500 Pa.

models. In the high asymptotic pressure case (see Fig. 9), the region of thermal equilibrium is clearly evident; it extends from the stagnation point up to the angular position $\theta \cong 20$ deg. Notice that the three models predict the same translational temperature profile, but the harmonic–oscillator model with Millikan and White's[13] relaxation time still overestimates the thermal disequilibrium, although in a less emphasized manner with respect to the low asymptotic pressure case.

Flow Pattern past the Cylinder

The flow characteristics along the stagnation line and the cylinder wall are generally true also for the overall flow pattern past the cylinder. The three models predict basically the same

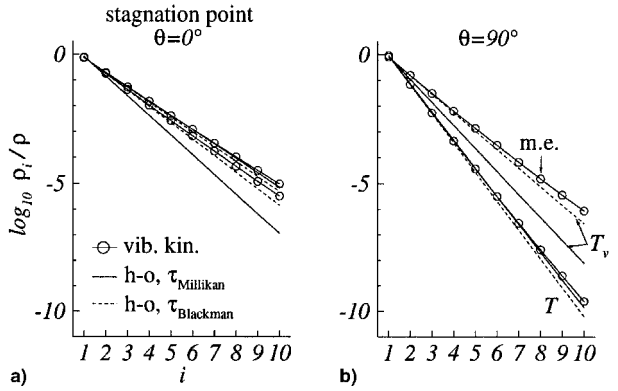

Fig. 6 Population distributions over the vibrational levels along the cylinder wall. p_∞ = 50 Pa.

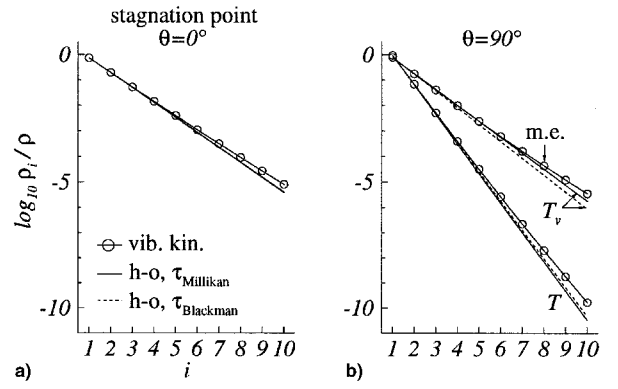

Fig. 7 Population distributions over the vibrational levels along the cylinder wall. p_∞ = 500 Pa.

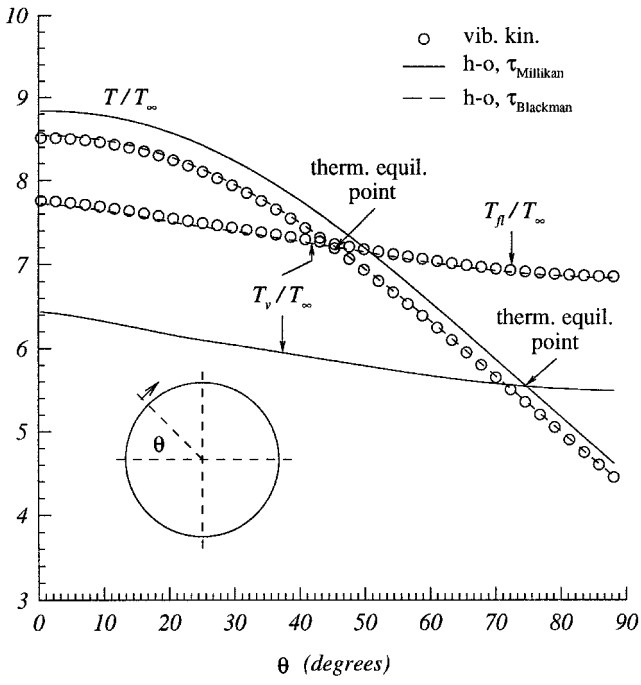

Fig. 8 Nondimensional translational, vibrational, and first-level temperature profiles along the cylinder wall. p_∞ = 50 Pa.

pressure field, but appreciable differences[17] are observed in the temperature fields between the harmonic-oscillator model with Millikan and White's[13] relaxation time and the other two models, which, instead, are in remarkable agreement.

The thermal disequilibrium pattern throughout the flowfield is illustrated in Figs. 10 and 11. These contour maps are con-

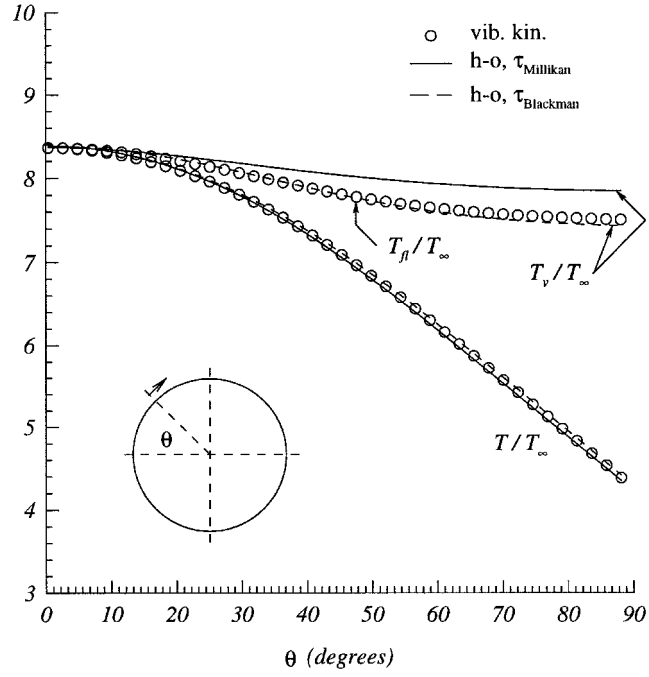

Fig. 9 Nondimensional translational, vibrational, and first-level temperature profiles along the cylinder wall. p_∞ = 500 Pa.

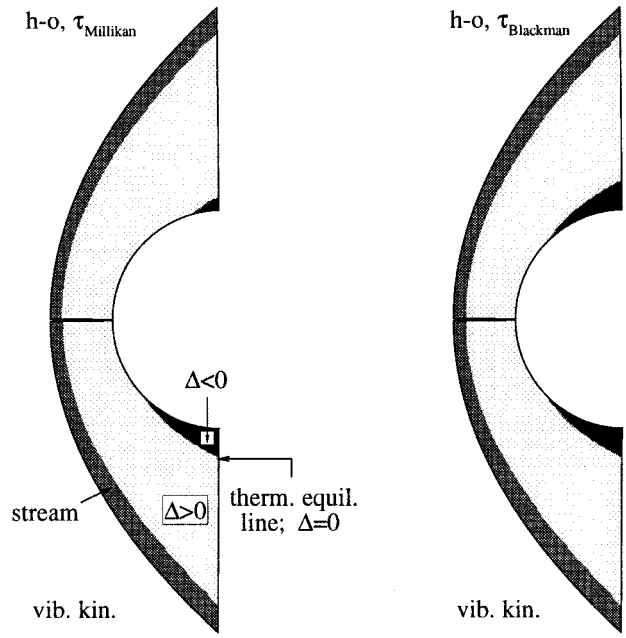

Fig. 10 Thermal disequilibrium pattern. p_∞ = 50 Pa.

structed by appropriately choosing the isolines of the parameter Δ, defined as

$$\Delta = 100[(T - T_v)/T] \tag{49}$$

for the two harmonic-oscillator models, and as

$$\Delta = 100[(T - T_{fl})/T] \tag{50}$$

for the vibrational kinetics model. In the low asymptotic pressure case (see Fig. 10), the region of thermal equilibrium reduces to a line in the flowfield through which the vibrational and first-level temperatures overshoot the corresponding translational temperatures. In the high asymptotic pressure case (see

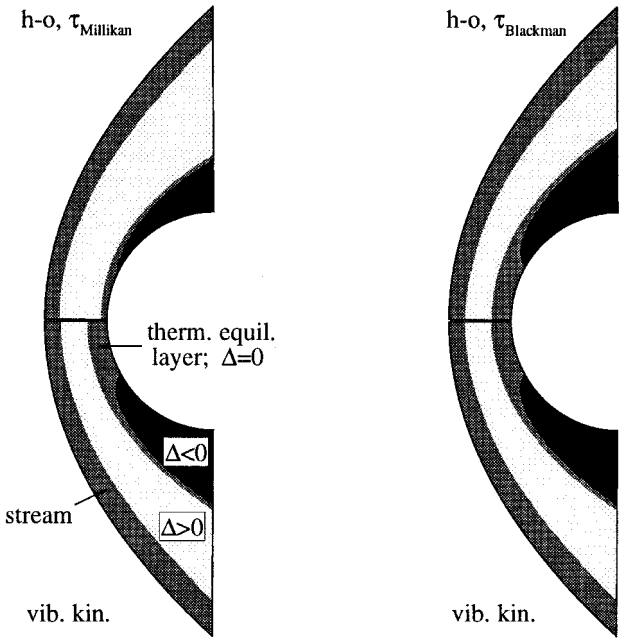

Fig. 11 Thermal disequilibrium pattern. p_∞ = 500 Pa.

Fig. 11), the region of thermal equilibrium has a relevant spatial extension centered about the stagnation point.

Conclusions

The results presented in this work have evidenced the basic Boltzmann behavior of the vibrational population distributions, although the harmonic-oscillator model with Millikan and White's[13] relaxation time shows some discrepancies with respect to the one with the Blackman's[14] relaxation time and the vibrational kinetics model; these latter models, in turn, are found in remarkable agreement.

However, caution should be exercised to generalize this conclusion to flow situations in which the differences between translational and first-level temperatures, in the vibrational kinetics model, are much larger than those found in the case studied here. It should be kept in mind that greater differences[2] in those temperatures are responsible for the strong non-Boltzmann character of the vibrational population distributions, as, for example, in flows expanding through a nozzle.

A further continuation of the research activity initiated with this work is to consider situations in which the N_2 molecules become chemically active and the dissociation-recombination processes assume an important role in determining the population distributions. Another interesting direction of the present research is to analyze the flow with the inclusion of viscosity and thermal conduction effects, because they should, supposedly, enhance a non-Boltzmann behavior of vibrational distributions in the vicinity of the cylinder wall.

Acknowledgments

This work has been partially supported by ASI (Agenzia Spaziale Italiana) and by the Regional Government of Sardinia. The authors acknowledge the courtesy of the Aerothermodynamics section of ESTEC (European Space Research & Technology Center) for providing the computing facilities.

References

[1]Meador, W. E., Miner, G. A., and Heinbockel, J. H., "Vibrational Relaxation in Hypersonic Flow Fields," NASA TP 3367, 1993.

[2]Cacciatore, M., Capitelli, M., De Benedictis, S., Dilonardo, M., and Gorse, C., "Vibrational Kinetics, Dissociation and Ionization of Diatomic Molecules Under Nonequilibrium Conditions," *Topics in Current Physics, Vol. 39: Nonequilibrium Vibrational Kinetics*, edited by M. Capitelli, Springer-Verlag, Berlin, 1986, pp. 5-46.

[3]Hansen, C. F., "Rate Processes in Gas Phase," NASA RP 1090, 1983.

[4]Capitelli, M., and Molinari, E., "Kinetics of Dissociation Processes in Plasmas in the Low and Intermediate Pressure Range," *Topics in Current Chemistry, Vol. 94: Plasma Chemistry III*, edited by S. Veprek and M. Venugopalan, Springer-Verlag, Berlin, 1980, pp. 59-109.

[5]Sharma, S. P., Ruffin, S. M., Gillespie, W. D., and Meyer, S. A., "Vibrational Relaxation Measurements in an Expanding Flow Using Spontaneous Raman Scattering," *Journal of Thermophysics and Heat Transfer*, Vol. 7, No. 4, 1993, pp. 697-703.

[6]Ruffin, S. M., and Park, C., "Vibrational Relaxation of Anharmonic Oscillators in Expanding Flows," *Journal of Spacecraft and Rockets*, Vol. 30, No. 1, 1993, pp. 59-68.

[7]Gillespie, W. D., Bershader, D., Sharma, S. P., and Ruffin, S. M., "Raman Scattering Measurements of Vibrational and Rotational Distributions in Expanding Nitrogen," AIAA Paper 93-0274, Jan. 1993.

[8]Sharma, S. P., Ruffin, S. M., Gillespie, W. D., and Meyer, S. A., "Nonequilibrium Vibrational Population Measurements in an Expanding Flow Using Spontaneous Raman Scattering," AIAA Paper 92-2855, July 1992.

[9]Sharma, S. P., "Rotational Relaxation of Molecular Hydrogen at Moderate Temperatures," AIAA Paper 92-2854, July 1992.

[10]Sharma, S. P., Ruffin, S. M., Meyer, S. A., Gillespie, W. D., and Yates, L. A., "Density Measurements in an Expanding Flow Using Holographic Interferometry," AIAA Paper 92-0809, Jan. 1992.

[11]Armenise, I., Capitelli, M., Celiberto, R., Colonna, G., Gorse, C., and Laganà, A., "The Effect of N + N_2 Collisions on the Non-Equilibrium Vibrational Distributions of Nitrogen Under Reentry Conditions," *Chemical Physics Letters*, Vol. 227, Nos. 1, 2, 1994, pp. 157-163.

[12]Armenise, I., and Capitelli, M., "On the Coupling of Non-Equilibrium Vibrational Kinetics and Dissociation-Recombination Processes in the Boundary Layer Surrounding an Hypersonic Reentry Vehicle," *Proceedings of the 2nd European Symposium on Aerothermodynamics for Space Vehicles*, European Space Agency, SP 367, ESTEC, Noordwijk, The Netherlands, 1995, pp. 287-292.

[13]Millikan, R. C., and White, D. R., "Systematics of Vibrational Relaxation," *Journal of Chemical Physics*, Vol. 39, No. 12, 1963, pp. 3209-3213.

[14]Blackman, V., "Vibrational Relaxation in Oxygen and Nitrogen," *Journal of Fluid Mechanics*, Vol. 1, 1956, pp. 61-85.

[15]Vincenti, W. G., and Kruger, C. H., Jr., *Introduction to Physical Gas Dynamics*, Krieger, Malabar, FL, 1965.

[16]Anderson, J. D., Jr., *Hypersonic and High Temperature Gas Dynamics*, McGraw-Hill, New York, 1989.

[17]Giordano, D., Bellucci, V., Colonna, G., Capitelli, M., Armenise, I., and Bruno, C., "Vibrationally Relaxing Flow of N_2 past an Infinite Cylinder According to State-to-State Vibrational Kinetics and to the Harmonic-Oscillator Model," AIAA Paper 95-2072, June 1995.

[18]Herzberg, G., *Molecular Spectra and Molecular Structure, I. Spectra of Diatomic Molecules*, D. Van Nostrand, Inc., New York, 1963.

[19]Huber, K. P., and Herzberg, G., *Constants of Diatomic Molecules*, Reinhold, New York, 1979.

[20]Capitelli, M., Gorse, C., and Billing, G. D., "V-V Pumping Up in Nonequilibrium Nitrogen: Effects on the Dissociation Rate," *Chemical Physics*, Vol. 52, No. 3, 1980, pp. 299-304.

[21]Billing, G. D., and Fisher, E. R., "VV and VT Rate Coefficients in Diatomic Nitrogen by a Quantum Classical Model," *Chemical Physics*, Vol. 43, No. 3, 1979, pp. 395-401.

[22]Doroshenko, V. M., Kudryavtsev, N. N., Novikov, S. S., and Smetanin, V. V., "Effect of the Formation of Vibrationally Excited Nitrogen Molecules in Atomic Recombination in a Boundary Layer on the Heat Transfer," *High Temperature (USSR)*, Vol. 28, No. 1, 1990, pp. 82-89.

[23]Swanson, R. C., and Turkel, E., "On Central-Difference and Upwind Schemes," *Journal of Computational Physics*, Vol. 101, No. 2, 1992, pp. 292-306.